Exploration of Tumor Biopsy Gene Signatures to Understand the Role of the Tumor Microenvironment in Outcomes to Lisocabtagene Maraleucel

N. Eric Olson[1,#], Seamus P. Ragan[1,#], David J. Reiss[1], Jerill Thorpe[1], Yeonhee Kim[1,#], Jeremy S. Abramson[2,3], Candice McCoy[1], Kathryn J. Newhall[1,#], and Brian A. Fox[1]

ABSTRACT

In the TRANSCEND NHL 001 study, 53% of patients with relapsed/refractory large B-cell lymphoma (LBCL) treated with lisocabtagene maraleucel (liso-cel) achieved a complete response (CR). To determine characteristics of patients who did and did not achieve a CR, we examined the tumor biology and microenvironment from lymph node tumor biopsies. LBCL biopsies from liso-cel–treated patients were taken pretreatment and ~11 days posttreatment for RNA sequencing (RNA-seq) and multiplex immunofluorescence (mIF). We analyzed gene expression data from pretreatment biopsies ($N = 78$) to identify gene sets enriched in patients who achieved a CR to those with progressive disease. Pretreatment biopsies from month-3 CR patients displayed higher expression levels of T-cell and stroma-associated genes, and lower expression of cell-cycle genes. To interpret whether LBCL samples were "follicular lymphoma (FL)–like," we constructed an independent gene expression signature and found that patients with a higher "FL-like" gene expression score had longer progression-free survival (PFS). Cell of origin was not associated with response or PFS, but double-hit gene expression was associated with shorter PFS. The day 11 posttreatment samples (RNA-seq, $N = 73$; mIF, $N = 53$) had higher levels of chimeric antigen receptor (CAR) T-cell densities and CAR gene expression, general immune infiltration, and immune activation in patients with CR. Further, the majority of T cells in the day 11 samples were endogenous. Gene expression signatures in liso-cel–treated patients with LBCL can inform the development of combination therapies and next-generation CAR T-cell therapies.

Introduction

The tumor microenvironment (TME) is an important predictor of outcomes in B-cell non-Hodgkin lymphoma (NHL). TME and tumor-associated macrophage stromal gene signatures have been associated with adverse outcomes to standard anthracycline and rituximab-based chemoimmunotherapy in patients with diffuse large B-cell lymphoma (DLBCL; ref. 1). The TME is also highly variable between different lymphoma subtypes and appears to impact prognosis and outcomes to novel immuno-oncology agents and targeted inhibitors (2–7). Pathogenesis of DLBCL involves evasion of immune recognition by T and natural killer cells as well as activation of immunosuppressive mechanisms [e.g., programmed cell death ligand 1 (PD-L1) pathway]. Multiple lymphoma studies have explored the role of the TME in response to checkpoint blockade (5, 8, 9). Specifically, the lymphoma TME has been described as exhibiting a spectrum between a more inflammatory environment such as in Hodgkin lymphoma, and a less inflammatory environment facilitating escape from immune surveillance observed in follicular lymphoma (FL) and DLBCL. On the basis of the relative responsiveness of these lymphomas to checkpoint inhibition, a more inflammatory TME has been associated with responsiveness to checkpoint inhibition (5).

How the TME affects CD19-directed chimeric antigen receptor (CAR) T-cell therapy is less well understood. Preclinical *in vitro* and *in vivo* evidence indicates that immunosuppressive macrophages can inhibit CAR T-cell function (10). Translational data from clinical B-cell NHL studies has shown that an inflammatory pretreatment TME with elevated CD3+ T cells correlated with response to CAR T-cell therapy (11–13).

Lisocabtagene maraleucel (liso-cel) is a CD19-directed, autologous 4-1BB co-stimulated CAR T-cell product administered at equal target doses of CD8+ and CD4+ CAR+ T cells (14). The TRANSCEND NHL 001 (TRANSCEND; NCT02631044) study enrolled patients with relapsed/refractory (R/R) large B-cell lymphoma (LBCL) who had progressed after two or more prior treatments. Eligible patients had DLBCL not otherwise specified (NOS), high-grade B-cell lymphoma with rearrangements of *MYC* and *BCL2* and/or *BCL6* (HGL), primary mediastinal B-cell lymphoma (PMBCL), LBCL transformed from indolent B-cell NHL, and grade 3B FL. Patients were heavily pretreated with a median of three prior lines of therapy, and two-thirds of patients were considered chemotherapy-refractory. The complete response (CR) rate after liso-cel treatment was 53%, with a low observed incidence of severe cytokine release syndrome (2%) and neurologic events (10%; ref. 15). Despite these encouraging results in a very high-risk patient population, and a probability of continued response at 2 years of 49.5% [95% confidence interval (CI), 41.4–57.0; ref. 16], not all patients achieve a CR or a durable response to liso-cel. Therefore, it is important to better understand what factors may influence response and durability.

Here, we examine tumor biopsies with associated long-term follow-up from a cohort of liso-cel–treated patients with LBCL to understand

[1]Bristol Myers Squibb, Seattle, Washington. [2]Massachusetts General Hospital Cancer Center, Boston, Massachusetts. [3]Harvard Medical School, Boston, Massachusetts.

[#]Affiliation at the time the study was conducted.

how the pretreatment TME may influence response. In addition, we identify changes in the posttreatment TME that are associated with the pretreatment TME and response.

Materials and Methods

Clinical efficacy

The efficacy outcomes of TRANSCEND have been reported previously (15). The primary efficacy endpoint was objective response rate, defined as the proportion of patients who achieved a best overall response (BOR) of CR or partial response (PR) based on assessment by the independent review committee (IRC) per Lugano 2014 criteria (17). Protocol-specified efficacy assessments occurred at 1, 3, 6, 9, and 12 months after liso-cel infusion, respectively, and then every 6 months thereafter until study completion. For this study, main analyses are based on the assessments of CR and progressive disease (PD) per IRC to focus on patient subgroups with the largest differences in response. For the analyses based on assessment time points of 1, 3, 6, 9, or 12 months, a patient is classified as CR if the assessment was CR at that time point, and PD if a patient had progressed at any time up to that time point. Most analyses compared patients who achieved and maintained a CR ($N = 27$) at 3 months (month-3 CR) to those with PD ($N = 32$) by 3 months (month-3 PD).

Patient biopsies

Needle biopsy samples were obtained from patients with R/R LBCL who were enrolled in the TRANSCEND study (**Table 1**). The first biopsy was obtained before lymphodepleting chemotherapy, which preceded liso-cel infusion [day < 0 pretreatment (PRE)] by 2 to 7 days. The PRE biopsy was required per protocol unless an archival biopsy with no intervening treatments was available. In many cases, the PRE biopsy was not available for RNA sequencing (RNA-seq) analysis because the quality or quantity of the sample was not sufficient or because the biopsy material was needed for protocol-required disease confirmation.

An optional biopsy was obtained 11 days (± 4 days) post-infusion [day 11 posttreatment (D11)], which was near the anticipated day of maximal liso-cel expansion. The D11 biopsy site was not necessarily the same location as the PRE biopsy site, as the site of both biopsies was at investigator discretion. Because the D11 biopsy depended on presence of accessible tumor, it could have led to a sample collection bias, so we compared the baseline characteristics of the patients with a D11 biopsy with those who had a pretreatment sample (**Table 1**).

The needle biopsy samples were formalin-fixed, paraffin-embedded (FFPE) material and were shipped to Charles River Laboratories or to Juno Therapeutics, a Bristol-Myers Squibb Company. Slides were cut from the FFPE blocks and were examined by a pathologist to determine and record the amount of tumor present, which was roughly 5 to 20 mm^2 and 20% to 100% tumor cell content, with most samples >60%.

In the TRANSCEND study (15), 269 patients with LBCL were infused with liso-cel and followed for a median of 12 months. Seventy-eight PRE samples and 73 D11 samples yielded quality RNA-seq data. To determine whether the RNA-seq study population was reflective of the full study population, we compared the response rates and progression-free survival (PFS) in the full study population with the patients in the PRE or D11 sets.

Institutional review boards at participating institutions (listed in Supplementary Appendix) approved the study protocol and amendments. The clinical study was done in accordance with the Declaration of Helsinki, International Conference on Harmonization Good Clinical Practice guidelines, and applicable regulatory requirements. All patients provided written informed consent for the use of biopsy material for analyses.

RNA-seq

At Q^2 Solutions/EA Genomics, RNA was extracted from slides or curls from FFPE biopsy material without macrodissection. After extraction, TruSeq RNA Exome kits (Illumina) were used to yield barcoded libraries and sequencing was performed using Illumina

Table 1. Patient and disease characteristics of those with RNA-seq samples.

	PRE (*N* = 78)	D11 (*N* = 73)
Sex, *n* (%)		
Male	55 (70.5)	50 (68.5)
Female	23 (29.5)	23 (31.5)
Age, *n* (%)	62 (56–69)	64 (59–70)
≥65 years	34 (43.6)	34 (46.6)
≥75 years	6 (7.7)	9 (12.3)
Histologic subtype, *n* (%)		
DLBCL, NOS	44 (56.4)	36 (49.3)
DLBCL, transformed from FL	18 (23.1)	14 (19.2)
DLBCL, transformed from other indolent NHL subtypes	4 (5.1)	9 (12.3)
High-grade B-cell lymphoma with gene rearrangements in *MYC* and either *BCL2*, *BCL6*, or both	9 (11.5)	8 (11.0)
Primary mediastinal B-cell lymphoma	1 (1.3)	4 (5.5)
FL grade 3B	2 (2.6)	2 (2.7)
ECOG PS at screening, *n* (%)		
0	35 (44.9)	34 (46.6)
1	40 (51.3)	37 (50.7)
2	3 (3.9)	2 (2.7)
Before lymphodepleting chemotherapy		
SPD^a (cm^2), median (IQR)	42.8 (20.1–95.1)	36.1 (19.1–98.0)
≥50 cm^2, *n* (%)	36 (46.2)	31 (42.5)
LDH (U/L), median (IQR)	351 (229–626)	290 (219–520)
≥500 U/L, *n* (%)	27 (34.6)	20 (27.4)
C-reactive protein (mg/L), median (IQR) at liso-cel infusion	59.6 (14.9–97.0)	32 (7.0–93.8)
Previous lines of systemic therapy, *n* (%)		
1 prior regimen	2 (2.6)	2 (2.7)
2 prior regimens	34 (43.6)	36 (49.3)
3 prior regimens	18 (23.1)	17 (23.3)
≥4 prior regimens	24 (30.8)	18 (24.7)
Chemotherapy refractory,^{b} *n* (%)	51 (65.4)	45 (61.6)
Prior HSCT, *n* (%)	27 (34.6)	19 (26.0)
Never achieved CR with previous therapy,^{c} *n* (%)	35 (44.9)	35 (48.0)
Secondary CNS lymphoma, *n* (%)	3 (3.9)	2 (2.7)

Abbreviations: CNS, central nervous system; ECOG PS, Eastern Cooperative Oncology Group performance status; HSCT, hematopoietic stem cell transplantation; IQR, interquartile range; LDH, lactate dehydrogenase; PRE, day <0 pretreatment; SPD, sum of the product of perpendicular diameters.
^{a}SPD was calculated per central review assessment before lymphodepleting chemotherapy. One patient with a PRE biopsy was not evaluable for SPD.
^{b}Refractory means no response to or PD after the last chemotherapy-containing regimen, or relapse <12 months after autologous HSCT.
^{c}Not only primary refractory but also refractory to subsequent lines of treatment.

HiSeq 2500 instruments. The target sequencing depth was 25 million paired-end reads for the first two batches and 50 million for the remaining four batches, with a sequencing length of 50 bp.

The quality of the reads in the fastq files was evaluated using FastQC (version 0.11.5). Illumina adapters were trimmed using cutadapt (version 1.15) and the resulting fastq files were used for downstream analyses. Sequence alignment was performed using STAR software (version 2.5.2b) using a two-pass mode and human genome reference hg38 (GENCODE GRCh38.p5 and the annotation from GENCODE Release 24). Counts were obtained using the quantMode GeneCounts option. Furthermore, the CAR sequence of liso-cel was joined to the genome so that the CAR sequence could be quantified. Alignments were evaluated using Picard tools (version 2.18) and samples with low-quality sequencing metrics were removed from analysis.

To assess how CAR T cells impacted the TME, PRE and D11 biopsies were compared. The final data set with passing quality RNA-seq data had 78 PRE samples and 73 D11 samples, with matching PRE and D11 samples for 30 patients.

Batch correction and differential expression analysis

The samples were collected and processed across six batches over 2.5 years. Although the key methodology was the same (sequencing vendor, library preparation kit, and Illumina sequencing technology), some procedures changed over time, including the total number of reads sequenced, the switch to a dual DNA/RNA extraction protocol, and the inclusion of samples with lower tumor fractions on the slides (Supplementary Table S1). Several batch correction approaches were explored by adding covariates to the DESeq2 (18) differential expression analysis (Supplementary Fig. S1) for the following key contrasts in this study: (A) CR versus PD at 3 months in the PRE samples and (B) D11 versus PRE. In both of those contrasts, using no batch correction yielded the highest number of differentially expressed genes. Adding a categorical covariate for six batches reduced the number of differential genes by ≥50% in the D11 versus PRE contrast. Batch 5 was all PRE samples and Batch 6 was mostly D11, so when they were treated as separate batches, the number of differential genes fell dramatically. Combining Batch 5 and Batch 6 preserved many of the D11 versus PRE differences. Several other covariates in the differential expression model were tested (e.g., percentage of tumor on slide, DV_{200}, batches), and the resulting fold-changes highly overlapped with the simple batch model (Supplementary Fig. S2). Given the above, all further analysis was performed using five batches (Batches 1–4 with 5 and 6 combined) as a covariate.

For sample level analyses, such as single sample gene set enrichment analysis (ssGSEA) scores and gene plot figures, we used the expression values adjusted by vst (DESeq2 R package; ref. 18), followed by removeBatchEffect (limma R package; ref. 19) for the five batch groups using the STAR counts as inputs. When performing differential expression analysis between two groups of samples, we used DESeq2 with the raw gene-level counts from the STAR output, with the five batch groups as a covariate. Supplementary Figure S3 shows the comparison of the fold-changes between response groups of the PRE samples.

Gene sets and enrichment analysis

For gene set enrichment analysis (GSEA; ref. 20), we used the clusterProfiler R package (version 3.14), which uses the R package fGSEA (21) internally and used 1,000 permutations to estimate the significance. With clusterProfiler, we searched the MSigDB (20) H (Hallmark; ref. 22) and C2 (Curated; ref. 20) gene sets as provided by the msigdbr R package (version 7.0.1). We used the GSEA module in

ArrayStudio (version 10; Qiagen) to complement the MSigDB-based approach. The EZH2 gene sets, NUYTTEN_EZH2_TARGETS (UP and DN; ref. 23), were identified in the MSigDB C2 and ArrayStudio analysis. Additional EZH2 gene sets were generated from a reanalysis of the Affymetrix microarray data for GEO Series GSE49284 (24), which included three lymphoma cell lines (WSU-DLCL2, KARPAS-422, and SU-DHL-6) that had been treated with and were sensitive to the EZH2 inhibitor EPZ-6438. The three cell lines were analyzed to identify the genes most downregulated or upregulated by EZH2 inhibition. The three individual lists were then merged and named the Knutson_EZH2_inhib (up and dn). Another pair of gene sets identified in the top MSigDB C2 results were the SHIPP_DLBCL_vs_FOLLICULAR_LYMPHOMA (UP and DN; ref. 25).

We added several other lymphoma-related gene sets to our analysis that have been used to characterize lymphoma biology or patient subsets: molecular high-grade signature (26), stromal-1 and -2 (1), activated B-cell versus germinal center B-cell (27), and double-hit positive versus negative (28). We added several immune-related solid tumor gene sets identified in recent publications: IFNγ, Thorsson/Institute for Systems Biology scores (29), and a melanoma T-cell exclusion signature (30).

With these gene sets, we calculated single-sample scores using ssGSEA (with the R package GSVA version 1.42.0). We compared two groups of samples using a Wilcoxon rank sum test (R 3.6.1; refs. 31, 32).

Lymphoma gene set scores and classifiers

To further explore the biologic differences between DLBCL and FL, we used a proprietary data set, plus NHL data from the International Cancer Genome Consortium (ICGC; https://dcc.icgc.org/releases/current/Projects/MALY-DE) and the Cancer Genome Characterization Initiative (CGCI; https://ocg.cancer.gov/programs/cgci/data-matrix). The proprietary data set was generated from commercially sourced FFPE samples (Avaden Biosciences): 70 DLBCL and 61 FL samples with RNA-seq performed using the same methods as applied to the liso-cel study samples. For the public data sets, ICGC had 40 DLBCL and 41 FL samples, while CGCI had 105 DLBCL and 13 FL samples.

We performed differential expression analysis with the commercially sourced DLBCL and FL samples and selected the top 200 genes for FL and 200 for DLBCL (Supplementary Table S2). These two gene lists were used to calculate ssGSEA scores for each sample and named FL_vs_DLBCL (genes higher in FL than DLBCL) and DLBCL_vs_FL (genes higher in DLBCL than FL). The two ssGSEA scores were combined to form a composite score (FL_like_score or FL-like score) by subtracting the DLBCL_vs_FL score from the FL_vs_DLBCL score.

In a prior study from the sponsor (33), a DLBCL TME classifier was constructed to identify a DLBCL high-immune infiltration phenotype, referred to herein as the DLBCL TME classifier. We applied the RNA-seq version of the classifier algorithm to label samples as TME-classifier positive or TME-classifier negative; otherwise, we used the classifier confidence score as a continuous score for characterization. We also used the RNA-seq data to construct a score and perform classification for the cell of origin (COO; ref. 34) and double-hit gene expression status (28) using the methods described in those publications.

T-cell co-expression network

We used Pearson correlations to find genes in PRE samples that were correlated ($r > 0.8$) to several TME-related genes (CD3E, CD163, COL1A1), and iteratively added genes correlated to any of the new

genes converging to 1,051 genes. We then performed community detection based on label propagation (R/igraph; ref. 35) and selected the T-cell community, which had 42 genes. We used R/igraph for the network visualization and colored the nodes using the $\log_2$-fold change of either month-3 CR versus PD in the PRE samples or $CD8^+$ versus $CD4^+$ $\log_2$-fold change from a dataset of purified immune cells (GSE60424; ref. 36).

FL lasso classifier

We used the internal DLBCL and FL data sets to train an FL classifier using a lasso model (cv.glmnet in R; ref. 37) to predict whether an NHL sample has FL histology (Supplementary Fig. S4). The classifier was then tested on the CGCI and ICGC public data sets and yielded an area under the curve of the receiver operating characteristic curve of 0.93.

Core FL and DLBCL samples to use in the training were determined by removing outliers beyond the $0.9 \times$ interquartile range of both the FL-like and DLBCL-like ssGSEA scores to train the lasso classifier on the most confident samples. In the core training set, after removing the $0.9 \times$ interquartile range outliers, there were 57 DLBCL and 53 FL samples. A lasso model (using cv.glmnet in R; ref. 37) with 10-fold cross-validation (family = "binomial", standardize = T) was trained

on the core samples using the 5,000 genes with the highest standard deviation. This resulted in 30 nonzero coefficients at the minimum lambda. The ssGSEA-based FL-versus-DLBCL score was concordant with the lasso FL classifier for >85% of the PRE samples in this dataset (Supplementary Fig. S5).

Logistic regression and random forest

We used logistic regression and random forest models to compare importance of transformed FL (tFL) status and the FL-like gene signature with month-3 CR as the outcome. We used all 78 patients who had PRE tumor biopsy RNA-seq data and defined the binary outcome as a 1 if the patient was in CR at month 3 and used a 0 if the patient had any other outcome. When tFL was in the model, it was encoded as 1 if the patient was tFL and 0 otherwise. We show the different logistic regression models in Supplementary Table S3. The input signature scores for the random forest were reduced to a set of features with a Pearson correlation of <0.75. If scores in the starting set had a correlation or anticorrelation >0.75, then one of the scores was manually selected for input into the model (Supplementary Fig. S6A). The variable importance was determined and reported in Supplementary Fig. S6B using the mean decrease in the Gini coefficient where higher values are more important.
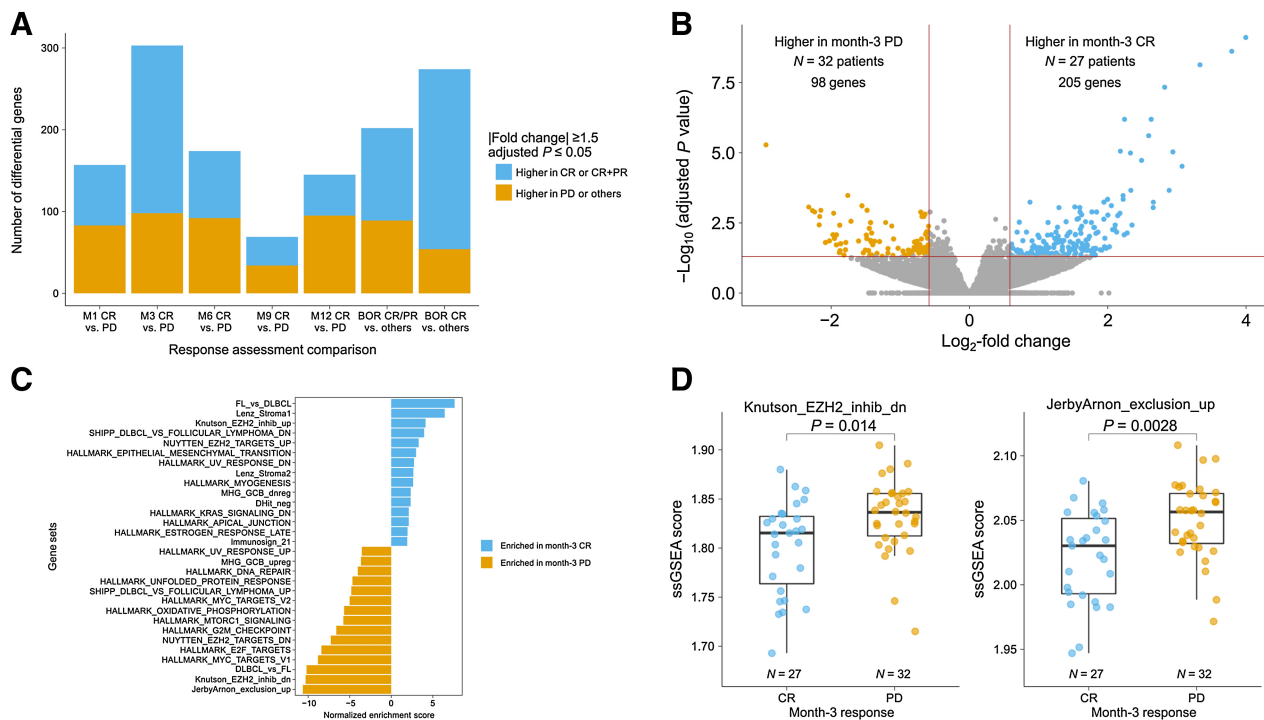
Figure 1.
Differential gene expression in pretreatment samples and gene sets associated with month-3 CR or PD. **A,** The height of the bar shows the number of differentially expressed genes when splitting the PRE samples into two groups based on various response assessments: CR versus PD at month-1, -3, -6, -9, or -12 or the BOR of CR/PR versus SD/PD or CR versus PR/SD/PD. In each bar, blue is the number of genes higher in patients achieving the noted response and orange is the number of genes for the noted nonresponse assessment. The numbers of samples in each comparison group are 38 (month 1), 59 (month 3), 62 (month 6), 63 (month 9), 60 (month 12), and all 78 samples were used in the BOR comparisons. **B,** Volcano plot of the contrast of month 3 CR versus month-3 PD in PRE samples. Orange points represent genes with higher expression in PRE samples of patients with month-3 PD, while blue points denote genes with higher expression in patients with month-3 CR. For both panels, a gene is labeled as differential if the fold change was more than ±1.5 (equivalent to a 0.585 $\log_2$-fold change) and the adjusted P value was less than 0.05 (threshold designated in panel B with red lines). **C,** The strongest GSEA scores comparing PRE samples of month-3 CR versus month-3 PD. Gene sets with a positive normalized enrichment score are associated with CR, while gene sets with a negative normalized enrichment score had a significant association with PD. **D,** ssGSEA scores for the EZH2 inhibitor gene set (Knutson_EZH2_inhib_dn) and the Jerby-Arnon T-cell exclusion gene set are shown for PRE samples, split into month-3 CR and month-3 PD, with the Wilcoxon P value shown above the groups.
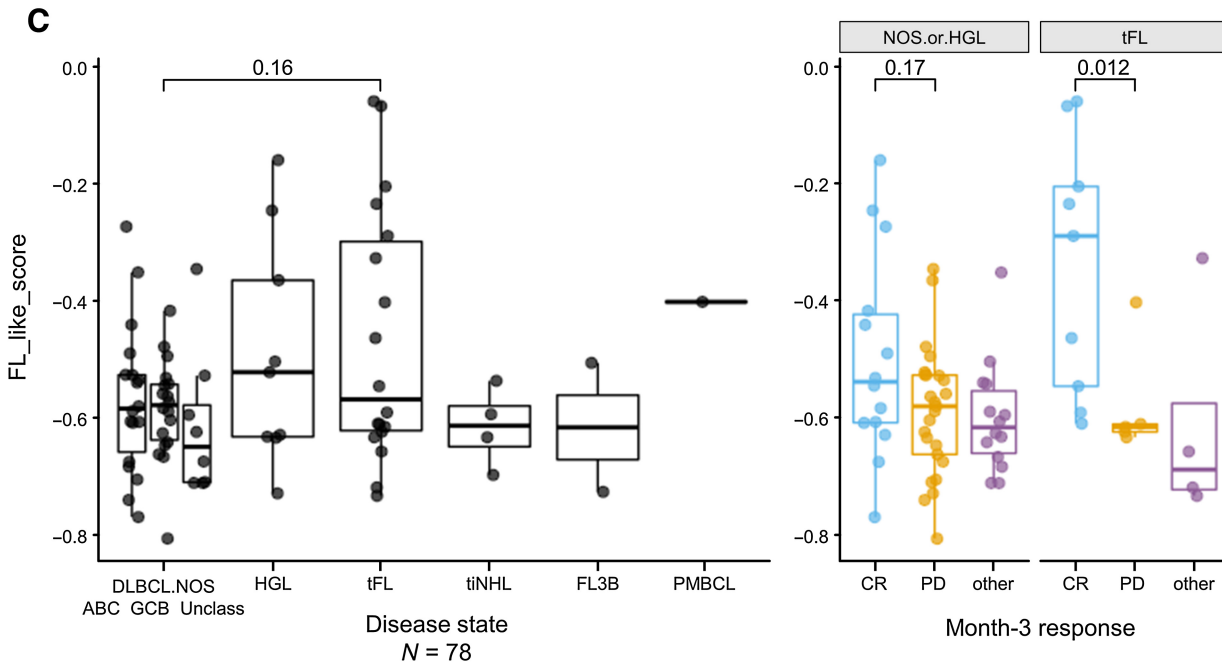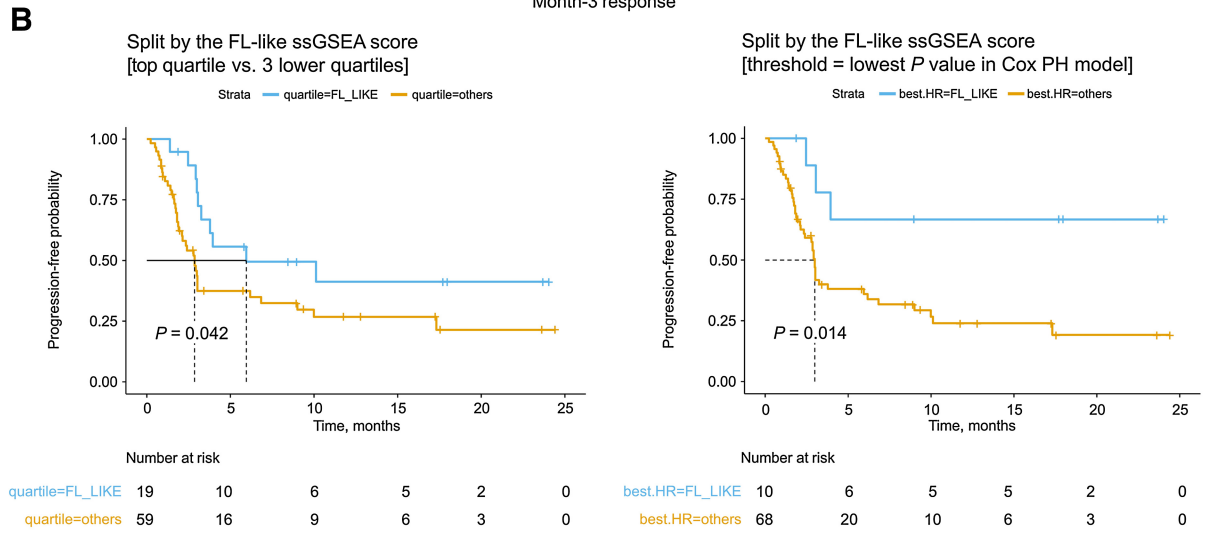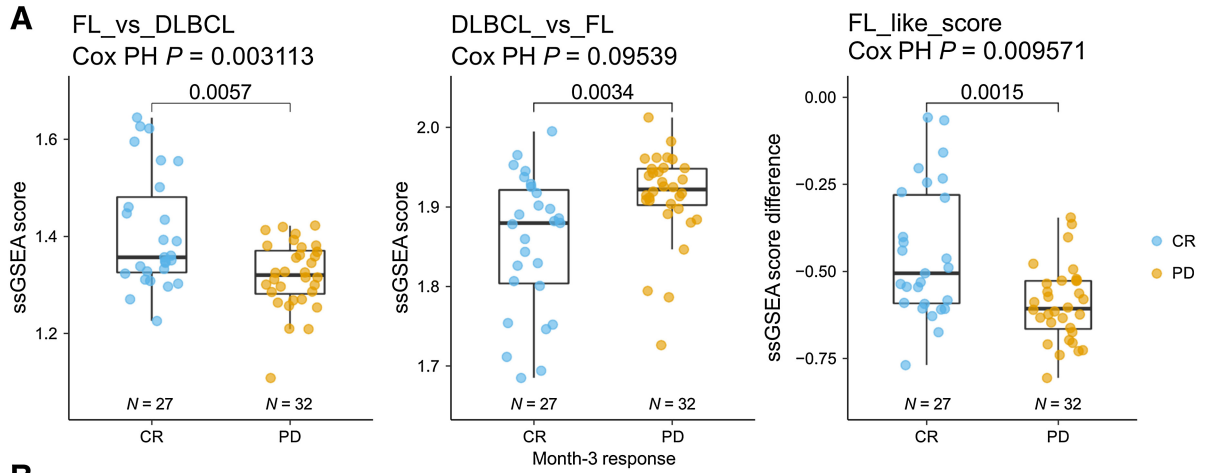
Survival analysis

Kaplan–Meier curves were used to visualize PFS differences between groups. Hazard ratios and Cox proportional hazard statistics were calculated using either a continuous covariate or discretized categorical variable. For the Kaplan–Meier curves using the FL_like_score score and the Risueño TME score, an optimized threshold between the two groups of patients was greedily determined by finding the most significant split by Cox proportional hazard likelihood ratio test.

Multiplex immunofluorescence

Three panels of five antibodies each were used to characterize the cellular content of the patient needle biopsy samples using multiplex immunofluorescence (mIF) with a PerkinElmer Vectra instrument as described previously (38, 39). Visiopharm was used to calculate the cell marker densities based on the hematoxylin and eosin–stained nuclei and marker intensities. Each panel was applied on a different slide; cell densities from each slide were analyzed independently (Supplementary Tables S4–S6).

The first panel had antibodies for the EGFR (to identify the CAR T cells that were engineered to have EGFR protein expressed), CD19, CD20, CD4, and CD8. The second panel had antibodies for CD73, FOXP3, IDO1, CD163, and PD-L1 and was originally intended to look for immune-suppressive pathways. The third panel had antibodies for EGFR, KI67, GZMB, CD3, and programmed cell death protein 1 (PD-1) and was intended to characterize the state of both the endogenous and CAR T cells.

For this study, regions of high background were manually excluded from analysis. Next, cells were segmented and phenotyped on the basis of individual algorithms to implement models that were qualitatively assessed, per fluorophore and per serial slide. These algorithms, implemented in Visiopharm, included preprocessing steps to reduce background noise and compute textural features (e.g., polynomial blob filters) to accentuate nuclei, membrane, or the entire cell where appropriate. After initial segmentation of cellular objects, a series of post-processing steps apply morphologic operations (e.g., erosion, dilation, splitting) and filtering on the basis of a combination of spatial properties (e.g., area, shape), preprocessed signal intensities, and textural information. Thus, the final cell marker positivity was not based simply on thresholding of raw signal intensity, but rather a series of filters and processing to maximize cellular signal relative to background noise. Where chromogenic immunohistochemistry was available, that was used as a gold standard to guide algorithm development for the mIF quantitation. That said, there were some samples where the signal-to-noise ratio was low for certain markers and the false negative rate high for those individual cases. Such cases were noted and if the signal-to-noise ratio was deemed too low, they were excluded from analysis.

The following combinations of markers were also used to calculate cell densities in cells/mm^2: KI-67$^+$CD3$^-$ [non–T-cell proliferation (we could not directly measure B-cell proliferation, as KI-67

and CD19 were not on the same panel)], CD3$^+$PD-1$^+$ (activated or exhausted T cells), CD3$^+$GZMB$^+$ (cytolytic T cells), and CD163$^+$PD-L1$^+$ or CD163$^+$IDO1$^+$ (activated macrophages). Differential analysis between groups of samples was performed using these markers or marker combinations with a Wilcoxon rank-sum test.

Data sharing

Bristol-Myers Squibb policy on data sharing may be found at https://www.bms.com/researchers-and-partners/independent-research/data-sharing-request-process.html. Data requests can be made using the link above. RNA-seq data for 14 of the 121 patients cannot be shared due to the informed consent agreement.

Results

PRE tumor biopsies exhibited gene expression differences associated with response

To identify gene expression differences in the PRE samples between responders and nonresponders, several definitions of response were explored. To focus on the differences between patient subgroups with the largest differences in response, we performed differential testing between PRE samples of patients who achieved a CR versus those with PD at defined time point response assessments of 1, 3, 6, 9, and 12 months. We additionally grouped patients by their BOR by comparing CR versus all other responses or CR/PR versus all other responses. Across those comparison groups, the highest number of differentially expressed genes in the PRE biopsies were found between patients who were in a CR at 3 months (month-3 CR) versus those who had PD by 3 months (month-3 PD; **Fig. 1A**). Although the number of differential genes from the comparisons varied, we found significant correlation between them (Supplementary Fig. S3). Using a ±1.5-fold change cutoff and a 0.05 FDR cutoff, 98 genes showed higher expression in PRE samples of patients with a month-3 PD ($N = 32$) and 205 genes had higher expression in PRE samples of patients with a month-3 CR ($N = 27$; **Fig. 1B**).

PD-associated gene sets were related to cell-cycle pathways

The full ranked list of genes from the differential test between month-3 CR and PD in the PRE samples was used for GSEA, which used gene sets from the Hallmark, lymphoma publications, and solid tumor signatures (**Fig. 1C**; Supplementary Table S7). The top normalized enrichment score for month-3 PD was from a gene set with higher expression in biopsies from patients with DLBCL versus patients with FL (DLBCL_vs_FL). Another gene set, Knutson_EZH2_inhib_dn, included genes that were downregulated by an EZH2 inhibitor applied to three DLBCL cell lines (GSE49284; ref. 24). Other gene sets included a variety of Hallmark gene sets related to various transcription regulators (e.g., MYC, E2F, MTORC1) and other proliferative and cell-cycle pathways (e.g., G2M and oxidative phosphorylation). For example, the EZH2 inhibitor and Jerby-Arnon T-cell exclusion (30) ssGSEA

Figure 2.
FL-like gene expression signature is associated with response and is higher in a subset of patients across NHL subtypes. **A,** These plots show the respective ssGSEA scores for the PRE samples with the patients split into two groups based on their Month 3 response. The *P* value of the Wilcoxon test is shown, along with the likelihood ratio *P* value from the Cox proportional hazard (PH) model for each score as a continuous predictor across all patients with PRE samples. **B,** Survival plots for the patients with LBCL with the top quartile of composite FL-like scores (top) and the optimal HR split (bottom). The log-rank *P* value is shown. **C,** The left plot shows the distribution of the composite FL-like ssGSEA score from PRE samples across the DLBCL subtypes: DLBCL NOS, FL3B (FL grade 3B), HGL, PMBCL, tiNHL (DLBCL transformed from indolent NHL), and tFL (DLBCL transformed from FL). The DLBCL NOS group is split into COO groups, as determined by gene expression: activated B cell (ABC), germinal center B cell (GCB), and unclassified (Unclass). The *P* value is showing the Wilcoxon test between all the samples in the DLBCL NOS group and the tFL group. The right side of panel C is showing the FL-like score on the *y*-axis and is splitting the samples by month-3 response and by disease state (DLBCL NOS or HGL on the left and tFL on the right), with the Wilcoxon *P* value comparing the CR and PD groups.

scores calculated for each sample were significantly higher in patients with month-3 PD (**Fig. 1D**).

CR-associated gene sets were related to FL-like, immune, and stromal gene sets

Several gene sets in the PRE samples were associated with month-3 CR (**Fig. 1C**). The top gene set in patients achieving a month-3 CR was a gene set derived from an independent set of FL and DLBCL samples and defined by genes with higher expression in FL (FL_vs_DLBCL). Therefore, the patients with a month-3 CR displayed a more FL-like tumor phenotype (**Fig. 2A**). **Figure 2B** shows the PFS curves when patients were divided into two groups based on the 25% of patients with the highest FL-like scores (19 FL-like vs. 59 others; log-rank $P = 0.042$) or with the optimal FL-like score threshold that resulted in the smallest Cox proportional hazards P value (10 FL-like vs. 68 others; log-rank $P = 0.014$). A gene expression–based lasso classifier was generated to label samples as FL-like, which gave similar results (Supplementary Figs. S4 and S5). Several LBCL biopsies with a high FL-like score had tFL; however, the FL-like score was also high in several DLBCL NOS and HGL samples, and about half of the tFL samples had a low FL-like score (**Fig. 2C**). Further, in samples from patients with tFL, the FL-like score was significantly higher in patients achieving month-3 CR compared with those with PD ($P = 0.012$); whereas, in patients with DLBCL NOS or HGL, the FL-like score only trended higher in patients with month-3 CR compared with those with PD ($P = 0.17$; **Fig. 2C**). In addition, the FL-like score had a stronger association with PFS in the tFL patients than the combined group of DLBCL NOS or HGL patients (Supplementary Fig. S6C). There was a trend toward more tFL patients with a high FL-like score (44%) than DLBCL NOS/HGL patients with a high FL-like score (19%, $P = 0.066$; Supplementary Fig. S6C). Finally, to directly compare tFL status and the FL-like gene expression score in predicting month-3 CR as the outcome, we performed several logistic regressions and random forest models (Supplementary Fig. S6A and S6B). We found that the FL-like score was more significant and had more importance in predicting month-3 CR than the tFL status (Supplementary Table S3).

The immune and stromal gene sets also showed higher expression in PRE samples from the month-3 CR patient group. The gene sets representing the Lenz stromal-1 and -2 signatures (1) and the Immunosign 21 signature (11, 12) were enriched in patients with month-3 CR (**Fig. 1A** and **C**). Some of the strongest individual genes with higher expression in PRE samples of patients in month-3 CR include *KLRB1*, *CD40LG*, *ICOS*, *CD28*, and *CCL21*. Consistent with the PD sets, one of the CR-associated gene sets was upregulated by EZH2 inhibition in DLBCL cell lines (24). Taken together, these results indicate the PRE tumor biopsies of patients with a month-3 CR following liso-cel therapy have a higher expression of immune and stromal-related genes than those with PD.

We constructed a co-expression network of T-cell–related genes to explore T-cell biology in the PRE samples (**Fig. 3**). For each gene in the network, we compared the association with CR to the $CD4^+/CD8^+$ expression ratios of the purified T-cell data gene set (36). Half of the network was more $CD4^+$-biased and had a stronger association with month-3 CR ($P = 0.049$). However, these analyses show that expression of $CD4^+$- and $CD8^+$-biased genes in the PRE biopsies were both associated with month-3 CR.

After liso-cel infusion, patients with CR had a greater increase in immune cell gene expression

Gene expression analysis of D11 post-infusion samples showed that expression of T-cell– and macrophage-related genes were higher in patients achieving month-3 CR compared with patients with month-3 PD. *CD3D* and the liso-cel CAR construct (**Fig. 4A** and **B**) plus macrophage-associated genes (e.g., *CD14*) were also generally higher in D11 samples of patients with month-3 CR and increased more from PRE to D11 in patients with month-3 CR (**Fig. 4C**). Other T-cell– and myeloid-expressed genes show a similar pattern to *CD3D* and *CD14* expression, respectively. B-cell genes (e.g., *CD19*) displayed a larger decrease at D11 in patients achieving month-3 CR (**Fig. 4D**).

### Cell-cycle gene sets were anticorrelated with PRE and D11 T-cell infiltration

Upon further exploration of the gene sets associated with month-3 CR, we found that pretreatment samples with high expression of cell cycle–related genes or genes positively regulated by EZH2 tended to have lower infiltrating T-cell levels. To inform this relationship with T cells, we found that the *CD3E* gene was anticorrelated to the *EZH2* gene ($r = -0.32$), a panel of 5 proliferation-associated genes ($r = -0.36$), and the EZH2i ssGSEA score ($r = -0.43$; Supplementary Fig. S7A). Similarly, the EZH2i ssGSEA score had significant association with month-3 PD ($P = 0.014$), as did the *EZH2* gene ($P = 0.021$), and the 5 proliferation genes ($P = 0.032$; Supplementary Fig. S7B). In addition, we verified the relationship between *EZH2* and T-cell genes by replicating it in two additional public data sets with DLBCL and FL samples (Spearman ρ of -0.62 and -0.49 for ICGC and CGCI, respectively; Supplementary Fig. S7C).

To identify genes in the PRE samples that were associated with D11 T-cell or liso-cel CAR expression, we investigated correlations between PRE and D11 for 30 patient-matched samples. We first established a high correlation (Spearman ρ = 0.59) between the T-cell gene score and the liso-cel CAR in the D11 samples (Supplementary Fig. S8A). Next, using paired samples from patients with both a PRE and D11 sample, we calculated that *CD3E* in the PRE samples has a correlation (0.52) with the T-cell genes in the D11 samples, but a lower correlation (0.32) with the liso-cel CAR gene. Conversely, PRE levels of *EZH2* had a stronger anticorrelation with D11 liso-cel CAR (-0.22) than with D11 T cells (-0.04), and PRE levels of *CD14* had a positive correlation with D11 T cells (0.39), which was not as strong as the T-cell correlation (Supplementary Fig. S8B).

To characterize the PRE genes most associated with D11 T-cell and liso-cel infiltration, we sorted the PRE genes by average correlation with D11 T-cell and liso-cel CAR genes from the 30 patient-matched samples and then performed a GSEA (Supplementary Fig. S8C). Overall, the gene set results are similar to those found when comparing month-3 CR versus month-3 PD PRE samples. For example, the DLBCL_vs_FL and Knutson_EZH2_inhib_dn gene sets were both enriched in the negatively correlated direction, consistent with those same gene sets enriched in the month-3 PD samples. However, the gene sets with the highest positive enrichment were the Lenz stromal-1 set, two EZH2i upregulated sets, the Hallmark IFNγ response set, and the FL-like set. The top gene sets were similar to the month-3 CR gene sets, although the Hallmark IFN sets here were not significantly enriched in the month-3 CR analysis.

Other lymphoma molecular features showed a mixed relationship with response and infiltration

Continuous scores or categorical classifiers were calculated for other DLBCL- and lymphoma-related molecular features and are summarized in Supplementary Fig. S6D and S6E. The Reddy COO score (34) and intrinsic apoptosis (40) scores were not associated with month-3 CR or PFS (Supplementary Fig. S6F). Notably, although only 11% of patients in this cohort were classified as HGL based on the presence of
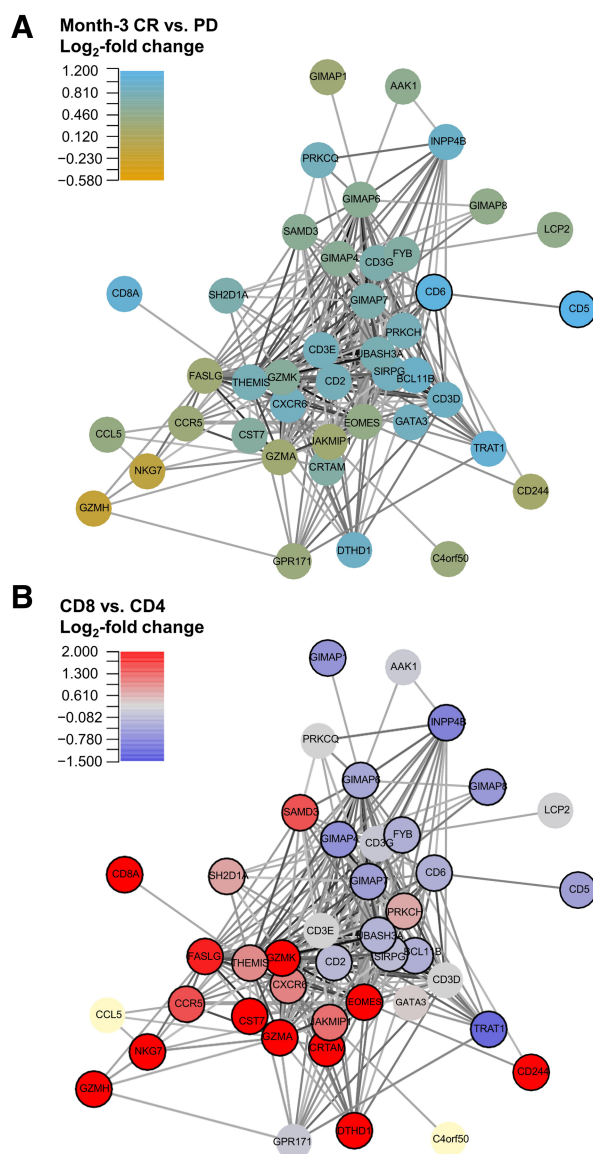
Figure 3.
T-cell correlation network in PRE samples. **A,** Circles are colored by the log$_2$-fold change difference between CR and PD at 3 months, with blue for genes which are higher in CR versus PD and yellow for genes higher in PD compared with CR. **B,** Circles in this plot have the same gene layout as (A) but are colored by the log$_2$-fold change between CD4$^+$ and CD8$^+$ cells from a public data set of CD4$^+$ and CD8$^+$ cells purified from blood (GSE60424). Blue indicates the gene was expressed higher in CD4$^+$ cells and red indicates the gene was expressed higher in CD8$^+$ cells. In both plots, gene nodes are outlined with a darker circle if that gene had a significant P value in the corresponding comparison.

gene rearrangements in *MYC* and either *BCL2*, *BCL6*, or both, 40% of patients had positive double-hit gene expression (ref. 28; Supplementary Fig. S6G), and those with positive double-hit gene expression had significantly shorter PFS (log-rank P = 0.0044; Supplementary Fig. S6H). The recently described DLBCL TME classifier (33) did not show a different PFS when using the published threshold (Supplementary Fig. S6I), but if a new threshold was used that optimally split the patients into TME+ and TME−, then the patients with a TME+

phenotype had a significantly longer PFS (log-rank P = 0.011), and the continuous probability score suggested that patients with a low TME score were enriched for nonresponders (Supplementary Fig. S6J and S6K). Although trending, neither the Immunosign 21 signature nor the death receptor signature (40) were significant in the month-3 CR versus PD comparison despite previous reports (11, 12).

mIF confirmed RNA-seq observations and additionally showed a large endogenous T-cell increase post-infusion

The PRE (N = 58) and D11 (N = 53) tumor biopsies were examined by mIF to further examine the immune cell subsets (38, 39). On average, for the samples with matched RNA-seq and mIF data, the correlation between gene expression and cell density was moderate to high (Supplementary Fig. S9A), as measured by Spearman ρ. The T-cell genes (*CD3D*, *PDCD1*, and *CD8A*) were highly correlated (0.62–0.73) with their respective T-cell marker densities. Macrophage-related markers (*CD163*, *PD-L1*, and *IDO1*) had a similar range of correlations (0.66–0.79). However, B-cell markers *CD19* and *CD20* had lower correlations: 0.39 and 0.58, respectively.

Examination of the measured cell densities in the PRE samples demonstrated that the T-cell association trends with CR were highest for PD-1$^+$ T cells using the month-1 assessment, while PD-1$^+$ T cells with later time point assessments and general CD3$^+$ cells (i.e., irre-spective of the PD-1$^+$ marker) did not trend with CR (**Fig. 5A**; Supplementary Fig. S9B). Conversely, a subset of CD163$^+$ macro-phages, those that were IDO1$^+$ or PD-L1$^+$, and proliferating tumor cells (measured as KI67$^+$ and CD3$^-$ cells) appeared to be higher in the PRE samples of patients with PD (**Fig. 5A**; Supplementary Fig. S9C and S9D).

In D11 biopsies, the EGFR marker was used to distinguish CAR T cells from endogenous T cells, with a correlation of 0.691 (Spearman ρ) between the liso-cel CAR gene expression in the RNA-seq data and the EGFR$^+$ cell density in the mIF data (Supplementary Fig. S9A). Both endogenous (EGFR$^-$) and CAR (EGFR$^+$) CD4$^+$ and CD8$^+$ cells were higher in D11 samples of patients achieving month-3 CR versus patients with PD (**Fig. 5B**). Furthermore, the CAR T cells comprised on average 5% of the T-cell density in the D11 samples (**Fig. 5B**).

Discussion

Although previous studies have described the influence of tumor and TME biology on CAR T-cell therapy outcomes, this is the largest study using both RNA-seq and mIF to examine the role of the pretreatment and posttreatment TME in patients with LBCL with long-term follow-up. On the basis of patient and disease characteristics of the PRE and D11 patient groups, the groups are generally similar to one another. The patient and disease characteristics of both groups are also similar to those of the overall study population as previously reported (15), except for numerically higher median C-reactive protein and lactate dehydrogenase in the PRE group and numerically higher proportion of the sum of the product of perpendicular diameters (SPD) ≥50 cm^2 in both the PRE and D11 groups (**Table 1**). The C-reactive protein is considered a measure of inflammatory state and lactate dehydrogenase and SPD are considered markers of tumor burden. The CR rate in patients with PRE and D11 RNA-seq samples was 47% and 59%, respectively, and, therefore, within the 95% CI of the CR rate reported for the overall population [CR rate of 53% (95% CI, 46.8–59.4; ref. 15]. Because the D11 biopsy requires accessible tumor, there is a concern that the patients with a D11 biopsy could have higher tumor burden compared with the PRE group. However, we found this not to be the case, as the D11 patient group had lower tumor burden
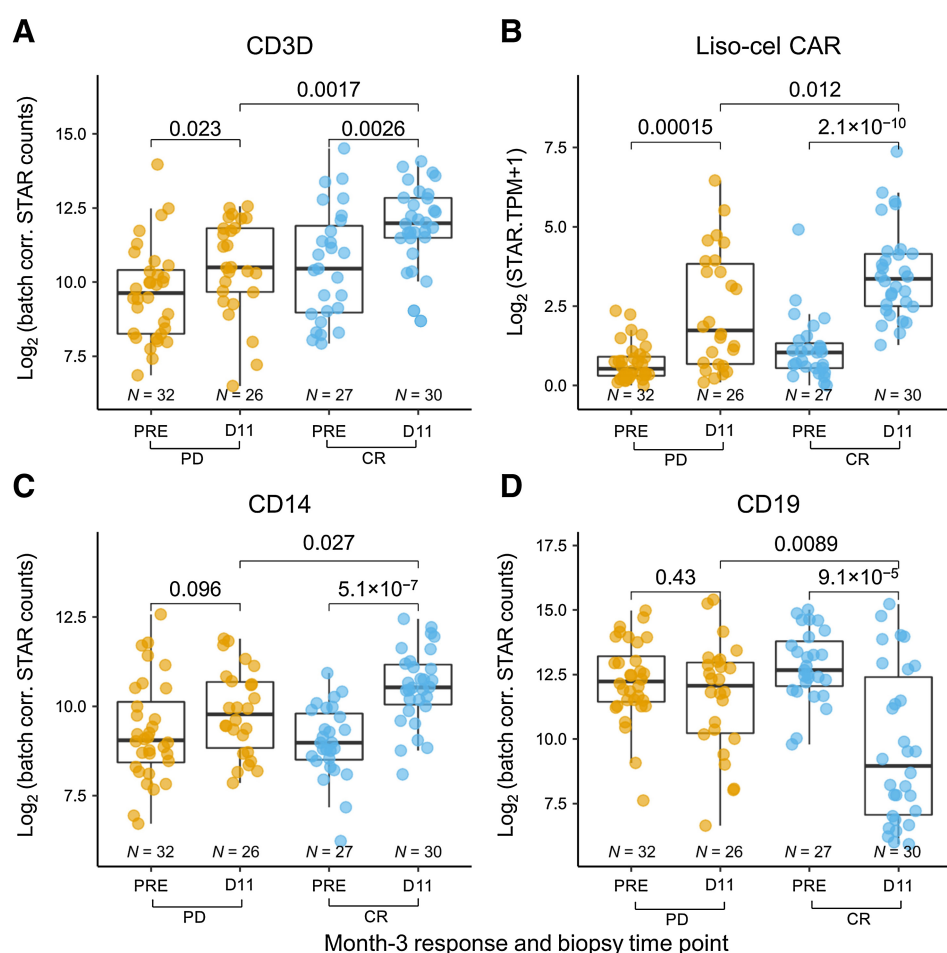
Figure 4.
Immune gene changes between PRE and D11 samples. **A–D,** CD3D, liso-cel CAR construct, CD14, and CD19 gene expression in PRE versus D11 samples and split by month-3 CR and PD. The P values were calculated using a Wilcoxon test. The liso-cel CAR construct plot used transcript per million values without any batch correction.

(numerically lower baseline SPD and lactate dehydrogenase) and better outcomes (higher CR rate) than the PRE group. In addition, the D11 patient group did not exhibit a different PFS from the full cohort (log-rank $P = 0.84$).

CR-associated biology

Some lymphoma subtypes (e.g., classical Hodgkin lymphoma and T-cell histiocyte-rich LBCL) have a paucity of lymphoma cells amidst a dominant polyclonal microenvironment and appear to have a better response to immune checkpoint blockade than DLBCL (5). In a study with 25 patients, Rossi and colleagues (12) observed elevated Immunosign 21 gene signature and Immunoscore (measure of intratumoral densities of CD3$^+$ and CD8$^+$ T cells; ref. 41) were associated with a CR to axicabtagene ciloleucel therapy. In a study of 10 patients that employed a different CD19 CAR T-cell therapy (JWCAR029; ref. 13), increased expression of immune-related chemokine receptors, adhesion molecules, and activated T cells were observed in patients with a CR versus PR. Our RNA-seq and mIF data indicate pretreatment levels of T cells are associated with better response, which is consistent with the results of prior studies.

The RNA-seq and mIF data allowed us to characterize the subtype and functional state of the TME immune cells. We found that PD-1$^+$ T cells in the PRE samples are trending as more associated with CR than total T cells (Supplementary Fig. S9D). However, no significant correlation was observed between BOR to tisagenlecleucel and PD-1$^+$ T cells (42). The T-cell correlation network analysis of the PRE samples

shows that both CD4$^+$ and CD8$^+$ genes are associated with month-3 CR (**Fig. 3**), although CD4$^+$ genes may be slightly more associated. In summary, the pretreatment state of T cells demonstrated that CD4$^+$, CD8$^+$, and PD-1$^+$ T cells may be important elements of the TME to support a positive response to treatment. In the PRE samples, the greater number of differential genes between CR and PD was found when using the month-3 assessment, which could imply that the tumor biology plays a larger role in the midterm response, whereas initial response (~1 month) and longer-term response (>12 months) may be more related to tumor burden, product composition, or longer-term CAR dysfunction or persistence.

D11 post-infusion samples showed increased immune infiltration (T cells and macrophages) in patients who developed a CR versus PD. In addition, in D11 biopsies, although infiltrating CAR T cells were associated with a CR, only approximately 5% of the T cells within the post-infusion biopsies were CAR T cells. This is similar to the percentage of CAR T cells reported with axicabtagene ciloleucel treatment in 17 patients (43). We and others (43) hypothesize that cytokines and other factors produced by CAR T cells invading the tumor result in an inflamed TME, enabling endogenous T cells and macrophages to aid in response.

We used the 30 patients with paired PRE and D11 samples to understand how pretreatment tumor biology may lead to D11 T-cell infiltration. As expected, there was a significant correlation between pretreatment levels of T-cell genes and post-infusion levels of CAR T cells and endogenous T-cell gene expression. However, the gene set in
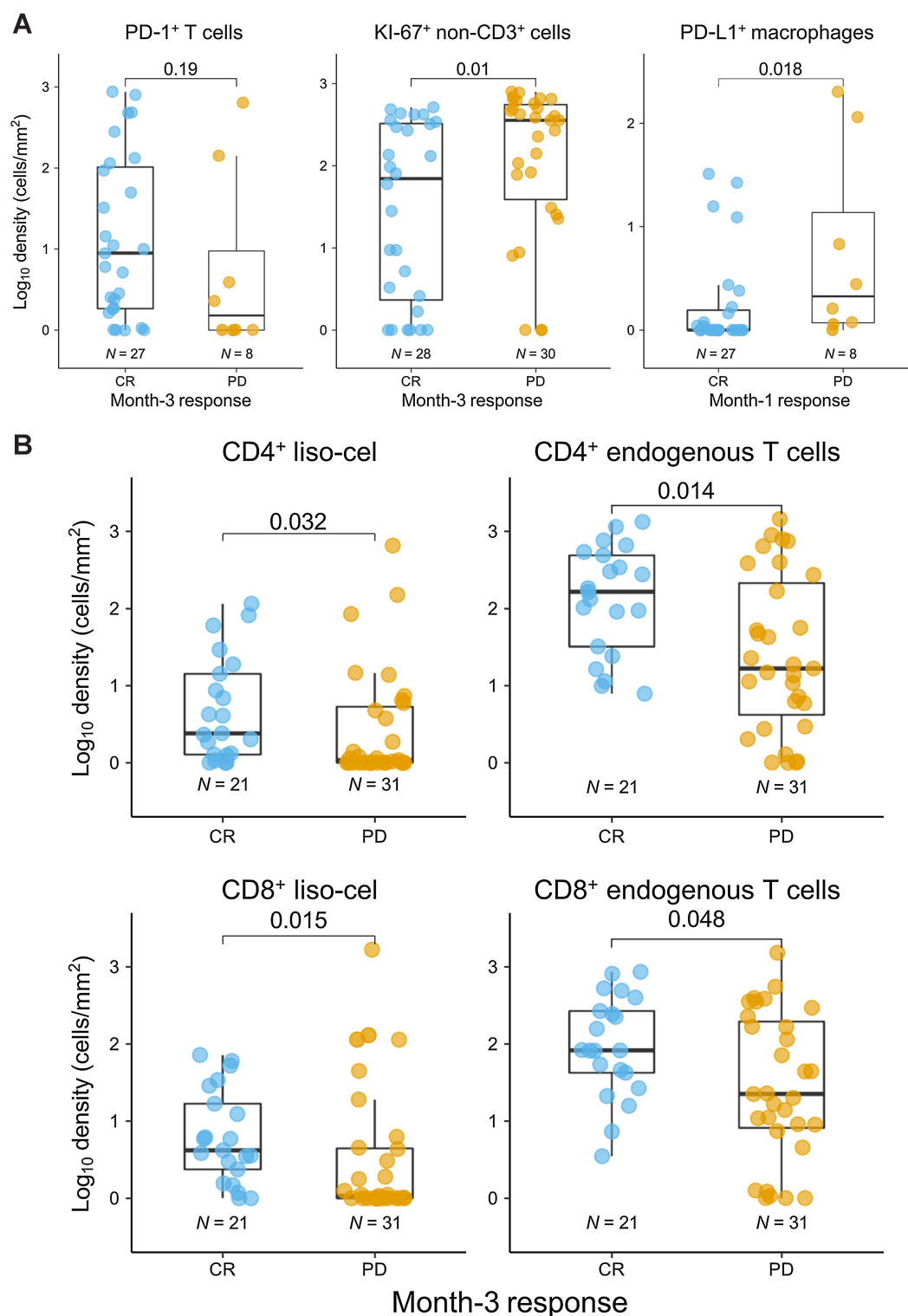
Figure 5.
Multiplex immunofluorescence. **A,** The left plot shows the cell density of PD-1$^+$CD3$^+$ cells from the PRE biopsies, split into two groups based on their month-1 response assessment (CR and PD); all other responses are excluded from the plot. The middle panel shows the cell density of KI-67$^+$ non–CD3$^+$ cells, split by the month 9 response assessment. The right panel shows the dual-positive PD-L1$^+$CD163$^+$ cells split by the month 9 response assessment. **B,** In the grid, the D11 cell densities for the CAR T cells (EGFR$^+$) are shown on the left and the endogenous T cells (EGFR$^-$) are shown on the right. The top plots are CD4$^+$ cells and the bottom plots are CD8$^+$ cells. The samples are split and colored by the month-3 response assessment. In all plots, the Wilcoxon P value is shown and the y-axis is log$_{10}$ cell density (cells/mm^2).

the PRE samples that was most correlated to the D11 T cells was the Lenz stromal-1 signature (Supplementary Fig. S8C). The stromal-1 signature is prognostically favorable in rituximab, cyclophosphamide, doxorubicin hydrochloride, vincristine sulfate, and prednisone treatment (1) and was also significantly enriched in this study in the PRE samples of patients achieving a month-3 CR (**Fig. 1C**). One aspect of stromal biology is exemplified by the higher expression of chemokines such as CCL21, a T-cell chemoattractant expressed by stromal cells that is related to T-cell trafficking in tumor-draining lymph nodes (44) but is also associated with migration of malignant lymphocytes (45, 46). In summary, a higher pretreatment level of T cells and stromal cells is correlated with increased immunity after liso-cel infusion and higher CR rates.

PD-associated biology

Liso-cel–treated patients with LBCL who had month-3 PD tended to have noninflamed tumors with higher levels of tumor cell proliferation. Using gene set enrichment, we found that EZH2 targets and transcription regulators (e.g., MYC, E2F, MTORC1, or other proliferative and cell-cycle pathways) were observed in patients with PD. We demonstrated that the proliferation and EZH2 target score in PRE biopsies were inversely correlated with T-cell gene expression in pretreatment and posttreatment biopsies in this study and other LBCL cohorts. Recent studies of lymphoma biopsies have shown DLBCL tumors have higher expression of proliferation genes than FL tumors (47). In addition, a double-hit gene expression signature (28) identified 40% of patients with a positive signature in this study, rather than 13% HGL as seen in the full study (15), and patients with this signature had shorter PFS. This is in contrast with the observation that the clinically determined HGL group had no significant difference in outcome in the full study. We also found that the melanoma tumor intrinsic gene set (30) was higher in DLBCL tumors where there were fewer T cells and where the patients had a worse month-3 response. In addition, the mIF data confirmed the RNA observation that PRE samples with higher tumor cell proliferation (i.e., non–T-cell KI-67$^+$) at pretreatment had worse response rates.

The DLBCL TME gene expression classifier was developed and shown to enrich for responders to the cereblon E3 ligase modulator (CELMoD) agent avadomide (CC-122; ref. 33). DLBCL TME classifier–positive samples were previously shown to have more stromal, macrophage, and/or T-cell content than classifier-negative samples, which had more B-cell and proliferative gene expression. We found that patients with very low TME classifier probability scores were more likely to progress, consistent with both the higher proliferation and reduced levels of stromal cells observed in the TME classifier–negative patients. In addition, despite the impact of COO on other LBCL therapeutic outcomes, there is not an association of COO with outcome in this cohort.

There are several drugs which could potentially change the tumor into a more favorable state for liso-cel or CAR T-cell infiltration and response. In lymphoma, EZH2 activity-enhancing mutations leads to increased cell proliferation and reduced antigen presentation (5). CDK4/6 inhibitors have been shown in both posttreatment clinical samples and mouse models to increase tumor immunity (48). Immunomodulatory drugs (IMiD) and CELMoD agents have been shown to increase IFN pathway genes in lymphoma cell lines (49) and in tumors after patients with DLBCL receive avadomide treatment (50). These observations suggest future experiments with EZH2 or CDK4/6 inhibitors, IMiDs, or CELMoDs to explore the interplay between tumor biology and the TME.

Impact of macrophages

Myeloid cells can have suppressive functions against CAR T cells (10). Yan and colleagues showed that 3 patients with higher levels of macrophage genes had PRs compared with 5 patients with CRs who had lower levels of macrophages (13). However, in Rossi and colleagues, patients with higher pretreatment levels of macrophage genes also had higher levels of T-cell and immune genes in general and were more likely to respond to treatment (12). In our study, we found the pretreatment gene expression patterns for myeloid markers were not associated with CR or PD. However, results obtained through mIF indicated that higher PD-L1$^+$ or IDO1$^+$ macrophages may trend towards being higher in PRE samples of patients with PD (**Fig. 5A**; Supplementary Fig. S9). This data, along with the observation that macrophages were more prevalent in D11 samples of patients with month-3 CR versus PD, suggest macrophages have both pro- and antitumor activity depending on their activation state. Thus, depletion of myeloid cells may be detrimental, and it may be more productive to alter the functional state of macrophages in LBCL prior to therapy to improve response to CAR T cells.

FL-like tumor biopsies

The observation that patients with a high FL-like gene expression pattern had a better response to liso-cel provides additional clues for understanding at least one of the mechanisms of response. To further understand FL-like gene expression, a more detailed look at FL biology is warranted. FL is characterized by tumor-infiltrating lymphocytes, including regulatory T cells and tumor-associated macrophages, and the tumor cells depend heavily on the TME for proliferation and survival (4). We identified a subset of patients with LBCL who exhibited an elevated FL-like gene expression signature that was associated with favorable outcomes in response to liso-cel. Although a high FL-like score was trending to be more common in patients with tFL, and the latter had a better outcome in the full study (15), the FL-like score was more important than tFL status in several statistical models of predicting CR at month 3. This suggests that FL-like gene expression is not exclusive to tFL and that it could play an important role in understanding response. The current data set suggests that an "FL-like" TME in LBCL is associated with favorable response to liso-cel therapy and provides the basis for further investigation of the association of pretreatment gene expression and response to liso-cel.

Limitations

Although the pretreatment gene expression data highlight some significant correlates for response, gaps remain in our full understanding of the role of the TME. Further analysis of the tumor biopsy signatures integrated with other patient factors, drug product features, or persistence of functional CAR T cells post-infusion may help inform a more complete view of the mechanisms of response and relapse. In addition, lymphoma tumor genetics, such as *PD-L1* structural variants or other tumor genetic alterations (*MYC, TP53, NFkB, NOTCH2, BCL2/6/10, FAS*), have been shown to help clarify the mechanisms of tumor immune escape (5), and tumor genetic data is not available for these patients.

Conclusion

This analysis identified novel gene expression signatures associated with response to liso-cel and provided insights into how tumor biology and the TME may affect response to liso-cel and CAR T-cell therapies in LBCL in general. These data will generate hypotheses to explore

additional combination therapy strategies and next-generation CAR T-cell therapies.

Authors' Contributions

N.E. Olson: Conceptualization, formal analysis, supervision, validation, writing–original draft, project administration, writing–review and editing. **S.P. Ragan:** Resources, data curation, formal analysis, validation, investigation, writing–original draft, writing–review and editing. **D.J. Reiss:** Conceptualization, formal analysis, writing–review and editing. **J. Thorpe:** Resources, methodology, project administration, writing–review and editing. **Y. Kim:** Formal analysis, methodology.

J.S. Abramson: Conceptualization, data curation, writing–original draft, writing–review and editing. **C. McCoy:** Methodology, writing–review and editing. **K.J. Newhall:** Conceptualization, resources, supervision, writing–original draft, project administration, writing–review and editing. **B.A. Fox:** Conceptualization, formal analysis, supervision, validation, visualization, writing–original draft, project administration, writing–review and editing.

Note

Supplementary data for this article are available at Molecular Cancer Therapeutics Online (http://mct.aacrjournals.org/).

References

1. Lenz G, Wright G, Dave SS, Xiao W, Powell J, Zhao H, et al. Stromal gene signatures in large B-cell lymphomas. N Engl J Med 2008;359:2313–23.
2. Cherkassky L, Morello A, Villena-Vargas J, Feng Y, Dimitrov DS, Jones DR, et al. Human CAR T cells with cell-intrinsic PD-1 checkpoint blockade resist tumor-mediated inhibition. J Clin Invest 2016;126:3130–44.
3. de Charette M, Houot R. Hide or defend, the two strategies of lymphoma immune evasion: potential implications for immunotherapy. Haematologica 2018;103:1256–68.
4. Fowler NH, Cheah CY, Gascoyne RD, Gribben J, Neelapu SS, Ghia P, et al. Role of the tumor microenvironment in mature B-cell lymphoid malignancies. Haematologica 2016;101:531–40.
5. Kline J, Godfrey J, Ansell SM. The immune landscape and response to immune checkpoint blockade therapy in lymphoma. Blood 2020;135:523–33.
6. Mulder TA, Wahlin BE, Österborg A, Palma M. Targeting the immune microenvironment in lymphomas of B-cell origin: from biology to clinical application. Cancer (Basel) 2019;11:915.
7. Rafiq S, Yeku OO, Jackson HJ, Purdon TJ, van Leeuwen DG, Drakes DJ, et al. Targeted delivery of a PD-1-blocking scFv by CAR-T cells enhances anti-tumor efficacy *in vivo*. Nat Biotechnol 2018;36:847–56.
8. Gravelle P, Burroni B, Péricart S, Rossi C, Bezombes C, Tosolini M, et al. Mechanisms of PD-1/PD-L1 expression and prognostic relevance in non-Hodgkin lymphoma: a summary of immunohistochemical studies. Oncotarget 2017;8:44960–75.
9. Wang Y, Wu L, Tian C, Zhang Y. PD-1-PD-L1 immune checkpoint blockade in malignant lymphomas. Ann Hematol 2018;97:229–37.
10. Ruella M, Klichinsky M, Kenderian SS, Shestova O, Ziober A, Kraft DO, et al. Overcoming the immunosuppressive tumor microenvironment of Hodgkin lymphoma using chimeric antigen receptor T cells. Cancer Discov 2017;7:1154–67.
11. Galon J, Rossi J, Turcan S, Danan C, Locke FL, Neelapu SS, et al. Characterization of anti-CD19 chimeric antigen receptor (CAR) T cell-mediated tumor microenvironment immune gene profile in a multicenter trial (ZUMA-1) with axicabtagene ciloleucel (axi-cel, KTE-C19). J Clin Oncol 2017;35:3025.
12. Rossi JM, Galon J, Chang E, Perbost R, Scholler N, Turcan S, et al. Pretreatment immunoscore and an inflamed tumor microenvironment (TME) are associated with efficacy in patients (Pts) with refractory large B-cell lymphoma treated with axicabtagene ciloleucel (Axi-Cel) in ZUMA-1 [abstract]. Cancer Res 2019;79:CT153.
13. Yan ZX, Li L, Wang W, OuYang BS, Cheng S, Wang L, et al. Clinical efficacy and tumor microenvironment influence in a dose-escalation study of anti-CD19 chimeric antigen receptor T cells in refractory B-cell non-Hodgkin's lymphoma. Clin Cancer Res 2019;25:6995–7003.
14. Ramsborg CG, Guptill P, Weber C, Christin B, Larson RP, Lewis K, et al. JCAR017 is a defined composition CAR T cell product with product and process controls that deliver precise doses of CD4 and CD8 CAR T cell to patients with NHL [abstract]. Blood 2017;130:4471.
15. Abramson JS, Palomba ML, Gordon LI, Lunning MA, Wang M, Arnason J, et al. Lisocabtagene maraleucel for patients with relapsed or refractory large B-cell lymphomas (TRANSCEND NHL 001): a multicentre seamless design study. Lancet 2020;396:839–52.
16. Abramson JS, Palomba ML, Gordon LI, Lunning MA, Wang M, Arnason JE, et al. Two-year follow-up of TRANSCEND NHL 001, a multicenter phase 1 study of lisocabtagene maraleucel (liso-cel) in relapsed or refractory (R/R) large B-cell lymphomas (LBCL). Blood 2021;138:2840.
17. Cheson BD, Fisher RI, Barrington SF, Cavalli F, Schwartz LH, Zucca E, et al. Recommendations for initial evaluation, staging, and response assessment of Hodgkin and non-Hodgkin lymphoma: the Lugano classification. J Clin Oncol 2014;32:3059–68.
18. Anders S, Huber W. Differential expression analysis for sequence count data. Genome Biol 2010;11:R106.
19. Ritchie ME, Phipson B, Wu D, Hu Y, Law CW, Shi W, et al. *limma* powers differential expression analyses for RNA-sequencing and microarray studies. Nucleic Acids Res 2015;43:e47.
20. Subramanian A, Tamayo P, Mootha VK, Mukherjee S, Ebert BL, Gillette MA, et al. Gene set enrichment analysis: a knowledge-based approach for interpreting genome-wide expression profiles. Proc Natl Acad Sci USA 2005;102:15545–50.
21. Korotkevich G, Sukhov V, Sergushichev A. Fast gene set enrichment analysis. bioRxiv 2019:060012.
22. Liberzon A, Birger C, Thorvaldsdottir H, Ghandi M, Mesirov JP, Tamayo P. The Molecular Signatures Database (MSigDB) hallmark gene set collection. Cell Syst 2015;1:417–25.

23. Nuytten M, Beke L, Van Eynde A, Ceulemans H, Beullens M, Van Hummelen P, et al. The transcriptional repressor NIPP1 is an essential player in EZH2-mediated gene silencing. Oncogene 2008;27:1449–60.

24. Knutson SK, Kawano S, Minoshima Y, Warholic NM, Huang KC, Xiao Y, et al. Selective inhibition of EZH2 by EPZ-6438 leads to potent antitumor activity in EZH2-mutant non-Hodgkin lymphoma. Mol Cancer Ther 2014;13:842–54.

25. Shipp MA, Ross KN, Tamayo P, Weng AP, Kutok JL, Aguiar RC, et al. Diffuse large B-cell lymphoma outcome prediction by gene-expression profiling and supervised machine learning. Nat Med 2002;8:68–74.

26. Sha C, Barrans S, Cucco F, Bentley MA, Care MA, Cummin T, et al. Molecular high-grade B-cell lymphoma: defining a poor-risk group that requires different approaches to therapy. J Clin Oncol 2019;37:202–12.

27. Lenz G, Wright GW, Emre NC, Kohlhammer H, Dave SS, Davis RE, et al. Molecular subtypes of diffuse large B-cell lymphoma arise by distinct genetic pathways. Proc Natl Acad Sci USA 2008;105:13520–5.

28. Ennishi D, Jiang A, Boyle M, Collinge B, Grande BM, Ben-Neriah S, et al. Double-hit gene expression signature defines a distinct subgroup of germinal center B-cell–like diffuse large B-cell lymphoma. J Clin Oncol 2019;37:190–201.

29. Thorsson V, Gibbs DL, Brown SD, Wolf D, Bortone DS, Ou Yang TH, et al. The immune landscape of cancer. Immunity 2018;48:812–30.e14.

30. Jerby-Arnon L, Shah P, Cuoco MS, Rodman C, Su MJ, Melms JC, et al. A cancer cell program promotes T cell exclusion and resistance to checkpoint blockade. Cell 2018;175:984–97.e24.

31. Barbie DA, Tamayo P, Boehm JS, Kim SY, Moody SE, Dunn IF, et al. Systematic RNA interference reveals that oncogenic KRAS-driven cancers require TBK1. Nature 2009;462:108–12.

32. Hanzelmann S, Castelo R, Guinney J. GSVA: gene set variation analysis for microarray and RNA-seq data. BMC Bioinformatics 2013;14:7.

33. Risueno A, Hagner PR, Towfic F, Fontanillo C, Djebbari A, Parker JS, et al. Leveraging gene expression subgroups to classify DLBCL patients and select for clinical benefit from a novel agent. Blood 2020;135:1008–18.

34. Reddy A, Zhang J, Davis NS, Moffitt AB, Love CL, Waldrop A, et al. Genetic and functional drivers of diffuse large B-cell lymphoma. Cell 2017;171:481–94.e15.

35. Csardi G, MNepusz T. 2006 The igraph software package for complex network research. InterJournal, complex systems, 1965. Available from: https://igraph.org/.

36. Linsley PS, Speake C, Whalen E, Chaussabel D. Copy number loss of the interferon gene cluster in melanomas is linked to reduced T cell infiltrate and poor patient prognosis. PLoS One 2014;9:e109760.

37. Friedman J, Hastie T, Tibshirani R. Regularization paths for generalized linear models via coordinate descent. J Stat Softw 2010;33:1–22.

38. Reiss DJ, Do T, Kuo D, Gray VE, Olson NE, Lee C-W, et al. Multiplexed immunofluorescence (IF) analysis and gene expression profiling of biopsies from patients with relapsed/refractory (R/R) diffuse large B cell lymphoma (DLBCL) treated with lisocabtagene maraleucel (liso-cel) in transcend NHL 001 reveal patterns of immune infiltration associated with durable response. Blood 2019; 134:202.

39. Swanson C, Do T, Merrigan S, Lonning S, Merriam K, Prentiss J, et al. Predicting clinical response and safety of JCAR017 in B-NHL patients: potential importance of tumor microenvironment biomarkers and CAR T-cell tumor infiltration. Blood 2017;130:194.

40. Singh N, Lee YG, Shestova O, Ravikumar P, Hayer KE, Hong SJ, et al. Impaired death receptor signaling in leukemia causes antigen-independent resistance by inducing CAR T-cell dysfunction. Cancer Discov 2020;10:552–67.

41. Galon J, Angell HK, Bedognetti D, Marincola FM. The continuum of cancer immunosurveillance: prognostic, predictive, and mechanistic signatures. Immunity 2013;39:11–26.

42. Schuster SJ, Bishop MR, Tam CS, Waller EK, Borchmann P, McGuirk JP, et al.; for the JULIET Investigators. Tisagenlecleucel in adult relapsed or refractory diffuse large B-cell lymphoma. N Engl J Med 2019;380:45–56.

43. Chen PH, Lipschitz M, Weirather JL, Jacobson C, Armand P, Wright K, et al. Activation of CAR and non-CAR T cells within the tumor microenvironment following CAR T-cell therapy. JCI Insight 2020;5:e134612.

44. Riedel A, Shorthouse D, Haas L, Hall BA, Shields J. Tumor-induced stromal reprogramming drives lymph node transformation. Nat Immunol 2016;17: 1118–27.

45. Hashikawa K, Yasumoto S, Nakashima K, Arakawa F, Kiyasu J, Kimura Y, et al. Microarray analysis of gene expression by microdissected epidermis and dermis in mycosis fungoides and adult T-cell leukemia/lymphoma. Int J Oncol 2014;45: 1200–8.

46. Hong CH, Lin SH, Lee CH. CCL21 induces mTOR-dependent MALAT1 expression, leading to cell migration in cutaneous T-cell lymphoma. In Vivo 2019;33:793–800.

47. Horn H, Kohler C, Witzig R, Kreuz M, Leich E, Klapper W, et al.; for the Molecular Mechanisms in Malignant Lymphomas (MMML) Network Project. Gene expression profiling reveals a close relationship between follicular lymphoma grade 3A and 3B, but distinct profiles of follicular lymphoma grade 1 and 2. Haematologica 2018;103:1182–90.

48. Goel S, DeCristo MJ, Watt AC, BrinJones H, Sceneay J, Li BB, et al. CDK4/6 inhibition triggers anti-tumor immunity. Nature 2017;548:471–5.

49. Hagner PR, Man H-W, Fontanillo C, Wang M, Couto S, Breider M, et al. CC-122, a pleiotropic pathway modifier, mimics an interferon response and has antitumor activity in DLBCL. Blood 2015;126:779–89.

50. Carpio C, Bouabdallah R, Ysebaert L, Sancho JM, Salles G, Cordoba R, et al. Avadomide monotherapy in relapsed/refractory DLBCL: safety, efficacy, and a predictive gene classifier. Blood 2020;135:996–1007.